Further Experiments on Supersonic Turbulent Flow Development in a Square Duct

D. O. Davis* and F. B. Gessner†
University of Washington, Seattle, Washington

The mean-flow structure of supersonic, turbulent, adiabatic-wall flow in a square duct is investigated experimentally over a development length of 50 duct widths for a uniform flow, Mach 3.9 condition at the duct inlet. The results show that a secondary flow cell structure develops that is similar to that for the incompressible case. This secondary flow distorts the primary flow, whose behavior also is influenced by shear-layer interaction effects as the wall boundary layers merge. Axial mean-velocity profiles plotted in terms of van Driest-scaled variables show that a well-defined log-law region exists in the near-wall layer. This region exists in the presence of a secondary flow that continuously modifies spanwise wall shear stress behavior along the length of the duct.

Nomenclature

a = duct half width, Fig. 7
a' = diagonal half width, Fig. 7
C = law-of-the-wall constant
C_f = skin friction coefficient, $2\tau_w/(\rho_e U_e^2)$
d_o = Preston tube outside diameter
d^+ = dimensionless Preston tube diameter, $d^+ = d_o U_\tau/\nu_w$
D = internal duct width
f = friction factor
f_c = incompressible flow friction factor
L = test section length
m = $[M_e^2(\gamma-1)/2]/[1+M_e^2(\gamma-1)/2]$
M = Mach number
P = pressure
Re' = unit Reynolds number, U_e/ν_e
$\overline{u'v'}$ = turbulent shear stress in xy plane
U = x component of velocity
U_τ = friction velocity, $(\tau_w/\rho_w)^{1/2}$
U^* = $(U_e/m^{1/2})\sin^{-1}(m^{1/2}U/U_e)$
V, W = y and z components of velocity, respectively
V_r = resultant transverse velocity
x = streamwise coordinate, Fig. 1
y,z = transverse coordinates, Fig. 7
y' = diagonal coordinate, Fig. 7
z_c = centered transverse coordinate, Fig. 7
β_k = pressure gradient parameter, $(\delta_k^*/\tau_w)dP/dx$
δ_k^* = $\int_0^\delta (1-U/U_e)/dy$
γ = specific heat ratio
κ = von Kármán's constant
ν = kinematic viscosity
ρ = density
τ = shear stress

Subscripts

e = boundary-layer edge
cl = centerline value
t = total or stagnation value
w = wall value

Presented as Paper 87-1287 at the AIAA 19th Fluid Dynamics, Plasma Dynamics, and Lasers Conference, Honolulu, Hawaii, June 8-10, 1987; received Feb. 8, 1988; revision received Aug. 22, 1988.

*Research Assistant, Department of Mechanical Engineering. Member AIAA.
†Professor, Department of Mechanical Engineering. Member AIAA.

Introduction

SUPERSONIC turbulent flow in a square duct is characterized by the growth of vortical flows in the cross plane (secondary flows) that alter the local flow structure from that observed for laminar flow conditions.[1,2] These secondary flows are generated by Reynolds stress gradients acting in the corner region and appear to have a cell structure similar to that observed for the incompressible case.[3,4] When the overall flow is supersonic, the flow develops in the presence of an adverse pressure gradient, whereas when the flow is incompressible, a favorable pressure gradient condition exists. It can be anticipated, therefore, that supersonic flow in a square duct will exhibit some features that are similar, yet others that are different, from those that exist when the flow is incompressible.

For the supersonic case, the duct behaves as a diffuser, and information on local flow development is of interest from the standpoint of understanding pressure recovery behavior in the duct. In the near entrance region, the developing flow is similar to that which exists in a rectangular supersonic aircraft inlet. For both applications, secondary flow is the dominant transport mechanism that influences wall shear stress rates and heat transfer behavior in the vicinity of a corner. The present study was initiated in order to gain a better understanding of how this secondary flow affects local flow conditions in a square duct over a development length longer than that considered in earlier studies.

Previous related work focused on experiments and predictions over a relatively short development length ($0 \le x/D \le 20$) for a Mach 3.9, uniform inlet flow condition.[5,6] The present experimental study was pursued in order to obtain and analyze data over a longer development length ($0 \le x/D \le 50$), which extends beyond the streamwise position where the boundary layers on opposite walls initially merge (nominally at $x/D = 30$). The results apply for the same inlet operating conditions as those prescribed in previous related work[5,6] and include total pressure, Mach number, and mean velocity profiles at four streamwise locations. Spanwise wall shear stress distributions and van Driest-scaled velocity profiles also are presented in order to examine the extent of near-wall similarity in the corner region.

Experimental Program

Flow Facility

The overall flow facility is the continuous flow, open-circuit wind tunnel described by Gessner et al.[5] For the present series of measurements, the original test section between the convergent-divergent nozzle and the test chamber was replaced by the segmented configuration shown in Fig. 1. This

configuration consists of an inner square duct (25.4 × 25.4 mm) made of brass, which is centered within an outer square duct of varying cross section made of plexiglas. This "duct within a duct" configuration was built to ensure a "clean" starting condition for the inner duct flow by allowing the distorted flow that develops along the sidewalls of the nozzle (cf. Fig. 2 of Ref. 5) to be bypassed through the annular space between the inner and outer ducts. The core flow at the nozzle exit was spatially uniform, thus yielding a low turbulence level, uniform flow condition at the inner duct inlet. The total pressure and total temperature at this location were 416 kPa and 300 K, respectively, when the tunnel was in operation.

For the specified inlet operating conditions ($M_i = 3.9$, $Re_i' = 2 \times 10^7 \text{m}^{-1}$), turbulent boundary-layer development was initiated at, or very near, the wedge-shaped leading edge of the inner duct (2-deg wedge angle), and wave effects in the duct were very weak, inasmuch as the inner duct wedge surface on each wall was aligned with the primary flow direction, as shown in Fig. 1. (This is a corrected value in comparison to that given in Refs. 1, 5, and 7. In those references, the values $Re_i' = 1.2 \times 10^6\ \text{m}^{-1}$ and $1.8 \times 10^6\ \text{m}^{-1}$, where they appear, should be replaced by $Re_i' = 1.3 \times 10^7\ \text{m}^{-1}$ and $2 \times 10^7\ \text{m}^{-1}$, respectively.) Previous temperature measurements with thermocouples embedded in the walls of the inner duct have indicated that the flow develops as an adiabatic-wall flow with a recovery factor of 0.89.[6] The local mean-flow structure observed in the present study thus corresponds to that of a supersonic, turbulent, adiabatic-wall flow in a constant area square duct that develops in the absence of strong internal waves from a low turbulence level, uniform mean-flow condition at the duct inlet.

Instrumentation and Data Reduction Procedures

The various types of pressure probes and data reduction procedures are the same as those used in previous related work.[5,6] Rather than attempting to deduce secondary flow behavior solely from measurements with a rotatable Conrad probe (Probe A in Fig. 2), an alternate rotatable probe also was used (Probe B) to minimize total pressure gradient effects on the data. Both probes were positioned at the exit plane of the duct, as shown in Fig. 1, and probe rotation was accomplished in minimum increments of 0.01 deg by means of an Ardel Kinamatic polar rotator (Model 19574) driven by a remote driver/control unit (Model 18556). A conical probe also was used for static pressure measurements in the flow. This probe had a 5-deg half-cone angle and a 1.07 mm body diameter, with 0.152 mm diam sensing holes (two) located ten body diameters downstream of the cone base. A circular pitot tube with an outside tip diameter of 0.305 mm was used to measure total pressure contours in the cross plane; wall and corner bisector total pressure values were determined by means of a flattened boundary-layer probe, with outer dimensions of 0.406 mm × 0.203 mm at the tip. Additional details of the probe configurations are given by Davis.[7]

Pressure probe data were taken at various x/D locations ($x/D = 20, 40, 50$) by adding or removing duct sections to the segmented configuration shown in Fig. 1 while maintaining the probe position fixed relative to the duct exit plane. Each probe was mounted on a remote-controlled, two-component micropositioner (Ardel Kinamatic Model 19557) that provided complete access to all points in the duct cross section. The sensing tip of each probe was located approximately 1 mm upstream of the duct exit plane. Additional data were taken at $x/D = 5.37$ by passing the probes through one of the support plates between the inner and outer ducts. Variable-length friction plates, acting as spacers between the inner and outer ducts, were used to match the static pressure of the inner and outer duct flows at the exit plane to the test chamber pressure before data were taken. This three-way match in pressure eliminated compression or expansion waves immediately downstream of the duct exit plane and, in turn, possible spurious effects on the data.

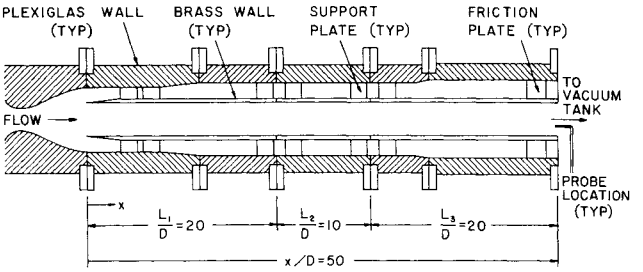

Fig. 1 Test section configuration.

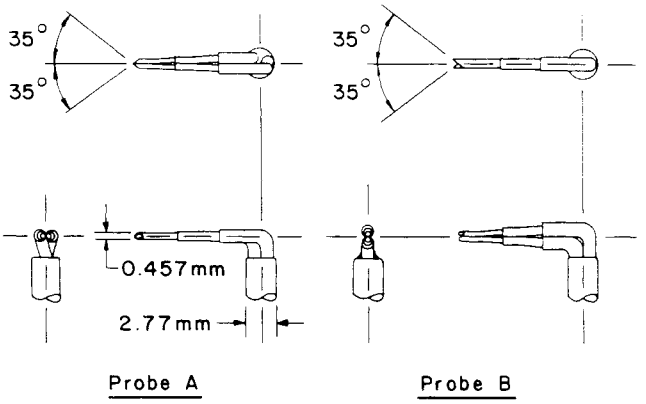

Fig. 2 Yaw angle probe configurations.

Results and Discussion

Preliminary Measurements

Total pressure contours were measured initially across the entire duct cross section at $x/D = 40$ in order to examine the extent of symmetry in the flow. The results are shown in Fig. 3 and indicate that the flow is locally symmetric about the corner and wall bisectors of the duct to within acceptable limits. The symmetric undulations that appear in the total pressure contours are similar to those that have been observed in incompressible square duct flow at the same streamwise location.[3,8] For incompressible flow conditions, these undulations are known to be caused by a secondary flow vortex pair centered about each corner bisector. For supersonic flow, the existence of these vortices was inferred from somewhat limited measurements in earlier related work.[1] In the present study, a concerted effort was made to measure these vortices directly.

In order to illustrate some of the difficulties associated with yaw probe measurements of secondary flow in a supersonic corner flow, two methods of measurement will be described. The first method is based on the use of Probe A in Fig. 2 alone, which normally would be adequate if the flow were incompressible. This probe was traversed across a quadrant of the flow, as shown in Fig. 4a, and the transverse velocity component in the z direction (W) was measured by rotating the probe about the y axis until a null differential pressure reading was obtained. At symmetrically positioned points about the corner bisector, such as (y_1, z_1) and (y_2, z_2) in Fig. 4a, where $y_2 = z_1$ and $z_2 = y_1$, the transverse velocities $W(y_1, z_1)$ and $W(y_2, z_2)$ were first measured directly (the solid components in Fig. 4a). Since the flow should be locally symmetric about the corner bisector, $V(y_2, z_2)$ and $V(y_1, z_1)$ were determined by employing the symmetry conditions $V(y_2, z_2) = W(y_1, z_1)$ and $V(y_1, z_1) = W(y_2, z_2)$. These V components are indicated by the dashed-line components in Fig. 4a. Resultant transverse flow vectors then were constructed by taking the vector sum of V and W at each measurement point in the cross plane.

The results of this approach for measurements with Probe A at $x/D = 50$ are shown in Fig. 4b. From the figure, it appears as if discrete vortices (secondary flows) are not actually present in the flow. It was recognized, however, that these results could have been influenced by total pressure gradients acting across the sensing holes of Probe A when the probe was located in region II of the quadrant shown in Fig. 4a and on the corner bisector. In order to investigate this possibility, additional data were taken with an alternate probe configuration (Probe B in Fig. 2) that minimized total pressure gradient effects in region II and along the corner bisector. The orientations of Probe B for these measurements are shown in Fig. 5a.

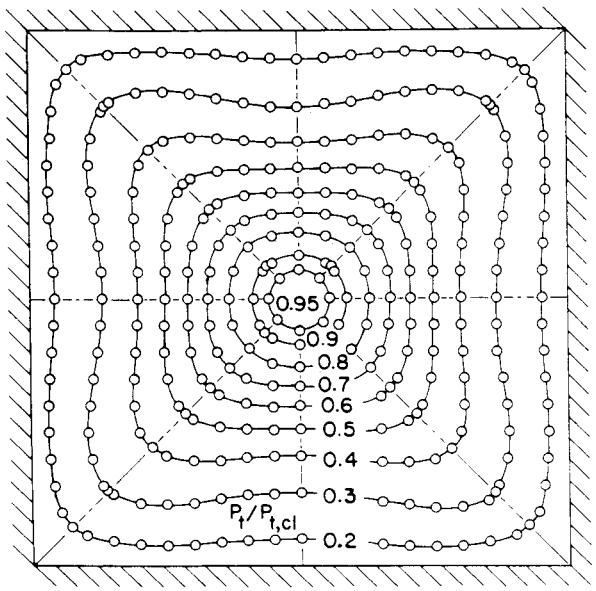

Fig. 3 Total pressure contours at $x/D = 40$.

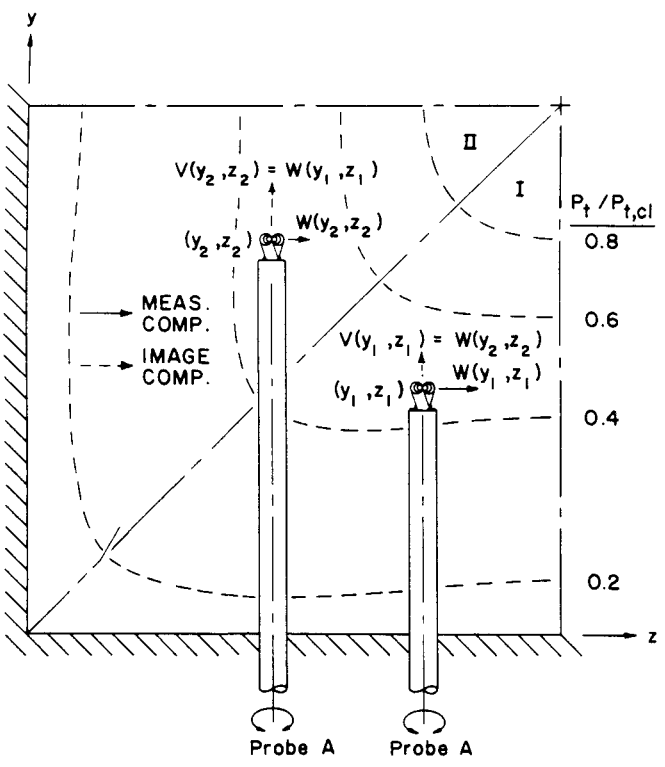

a) Probe positions

For these orientations, the resultant transverse velocity along the corner bisector was measured directly, and W values measured with Probe B in region II were coupled with W values measured with Probe A in region I in order to construct resultant transverse flow vectors elsewhere in the quadrant.

The results are shown in Fig. 5b, where two discrete secondary flow cells centered about the corner bisector now appear. The magnitude of the secondary flow $|V_r/U_{cl}| \leq 0.03$, is comparable to that which has been observed for the incompressible case.[3,4] The uncertainty in the magnitude of V_r/U_{cl} is estimated to $\pm$ 4%, exclusive of total pressure gradient effects on the measurements, which could not be quantified. The secondary flow pattern shown in Fig. 5b agrees well with the length-scale model predictions of Davis et al.[1] The additional vortices predicted by their model near a wall bisector appear, however, to be unrealistic, inasmuch as the existence of these vortices was not detected in the present study. On the basis of the results shown in Fig. 5b, it can be concluded that the distortion of the total pressure contours in Fig. 3 is the direct result of a secondary flow vortex pair centered about each corner bisector.

Static Pressure Development

Axial wall static pressure distributions measured along the inner and outer ducts for the $x/D = 40$ configuration are shown in Fig. 6. Also shown in this figure are line distributions based on one-dimensional flow theory and a modified friction factor that accounts for oblique shock wave effects induced by the wedge-shaped support plates between the inner and outer ducts.[9] Figure 6 shows that the adverse pressure gradient within the inner duct increases continuously along its length for matched pressure conditions at the duct exit plane. This figure also demonstrates the need for expanding sections along the outer duct in order to match the inner and outer duct static pressures at the exit plane. The slight undulations that appear in the distribution measured along the inner duct are the result of weak wave reflections in the inner duct.

Static pressure data also were taken with a conical probe along the axial centerline of the duct. These readings were consistently lower than corresponding wall static pressure readings (by 2, 8, and 3% at $x/D = 20$, 40, and 50, respectively). Although the data are limited, these results suggest that the

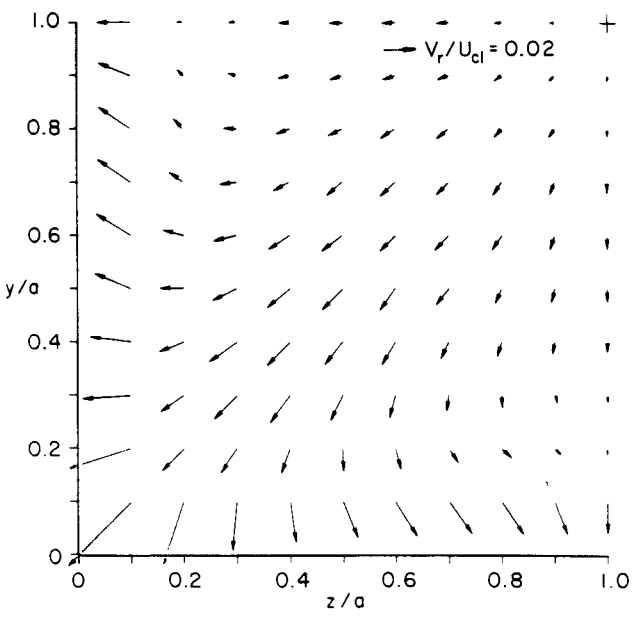

b) Transverse flow vectors at $x/D = 50$

Fig. 4 Transverse flow measurements with probe A.

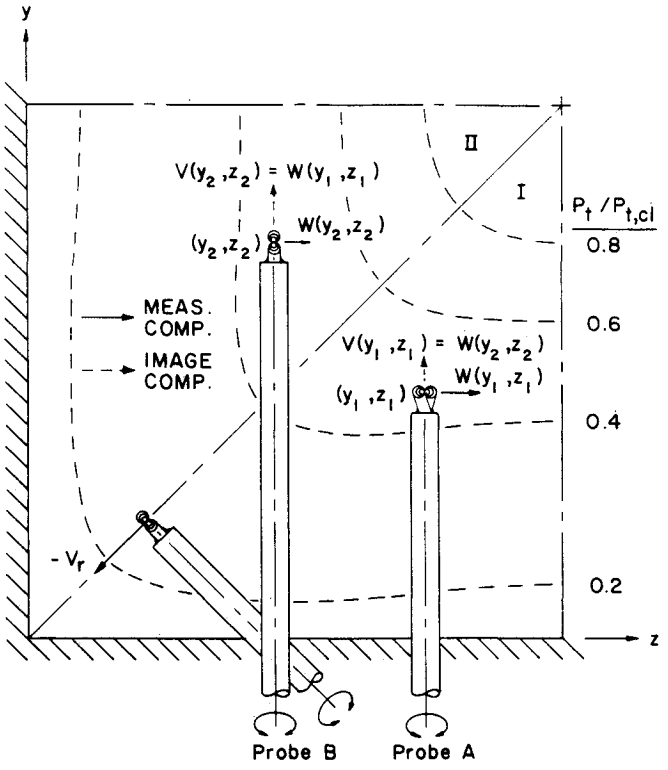

a) Probe positions

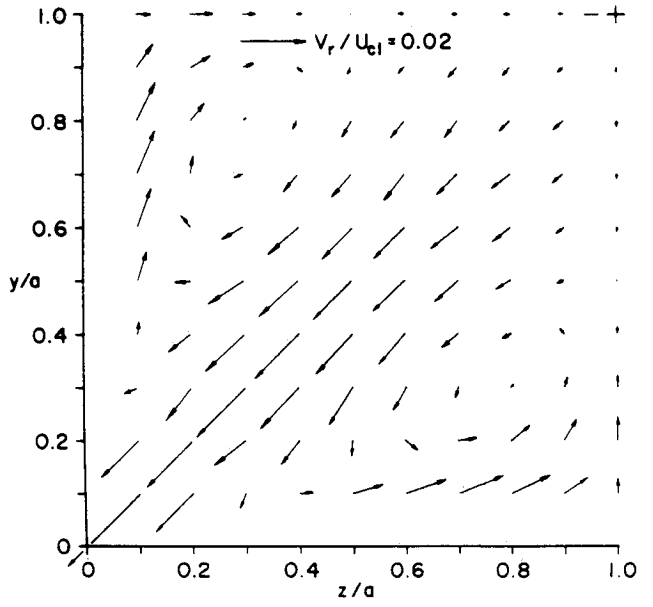

b) Transverse flow vectors at $x/D = 50$

Fig. 5 Transverse flow measurements with probes A and B.

core flow static pressure rise tends to lag the wall static pressure rise as the wall boundary layers merge (nominally at $x/D = 30$), but that this difference tends to diminish downstream. Static pressure profiles measured with the conical probe along the corner bisector of the duct at $x/D = 40$ exhibited a prominent peaking that was the result of a wall reflected shock originating at the probe tip. This same behavior has been observed by Om[10] for static pressure measurements with a conical probe in an adverse pressure gradient, supersonic boundary-layer flow. Inasmuch as accurate static pressure measurements could not be made at all grid points

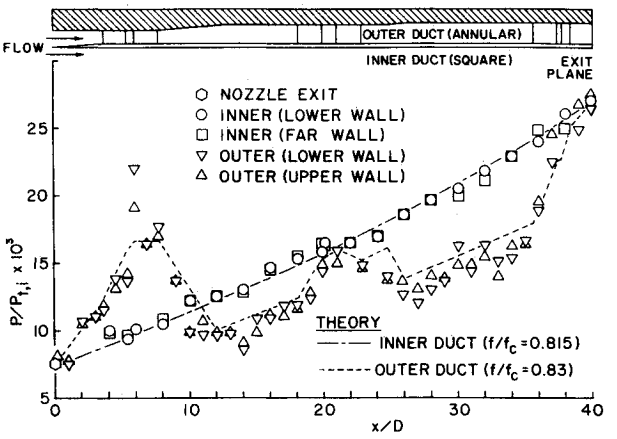

Fig. 6 Axial wall static pressure distributions.

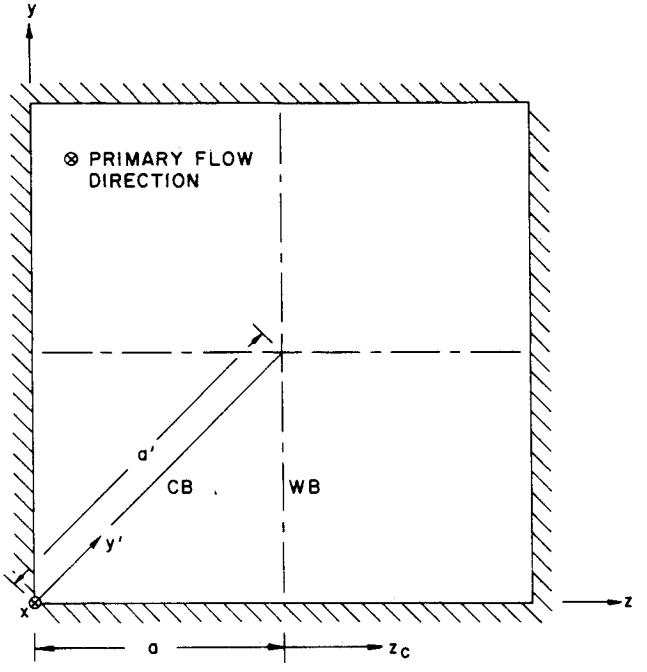

Fig. 7 Reference coordinates.

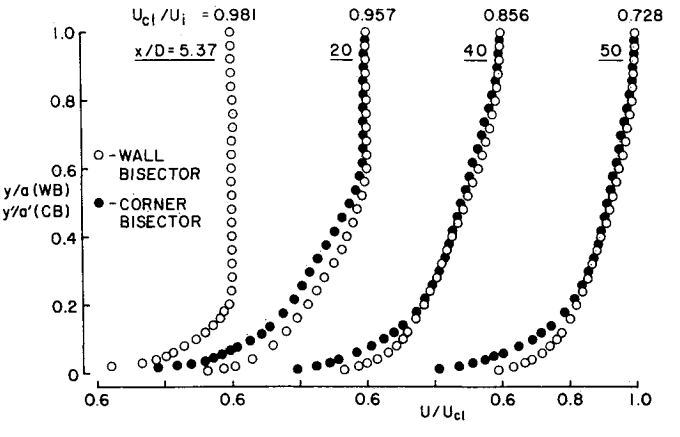

Fig. 8 Axial mean velocity profiles.

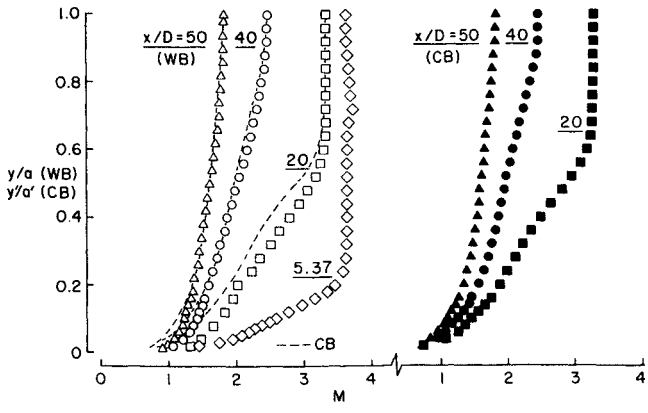

Fig. 9 Mach number profiles.

within the duct quadrant, subsequent stagnation pressure probe data were reduced by assuming a constant static pressure equal to the wall value at each streamwise location. This approach led to calculated U values on the axial centerline being underestimated by 0.3%, 1.8%, and 1.0% at $x/D=20$, 40, and 50, respectively. The corresponding underestimation in calculated M values at these locations was 1.0%, 4.1%, and 1.6%, respectively.

Primary Flow Development

In order to examine axial mean velocity and Mach number profile development, measurements were made along the wall bisector (WB) traverse shown in Fig. 7 ($0 \le y/a \le 1$, $z/a=1$) and along the corner bisector (CB) traverse corresponding to the y' coordinate shown in this figure ($0 \le y'/a' \le 1$). Axial mean velocity profiles measured at four streamwise locations ($x/D=5.37$, 20, 40, 50) are shown in Fig. 8. Along the centerline of the duct ($y/a=y'/a'=1$), the results show that the axial centerline velocity decreases monotonically in the presence of the increasing adverse pressure gradient shown in Fig. 6. This behavior is in contrast to that for the incompressible case, where the pressure gradient is favorable, and the axial centerline velocity first increases as the core flow accelerates, reaches a maximum as the wall boundary layers merge near $x/D=30$, and then decreases as the flow approaches a fully developed state.[8,11]

For supersonic square duct flow, Fig. 8 shows that the wall boundary layers have merged at $x/D=40$, so that a core flow no longer exists downstream of this location. Close observation of Fig. 8 also reveals that mean shear rates in the outer region of the flow at $x/D=40$ exceed those at $x/D=50$. This behavior is similar to that observed in incompressible square duct flow, where mean shear rates in the outer region at $x/D=40$ are greater than those further downstream as a result of shear layer interaction effects in the flow.[8] It would appear that this same mechanism is responsible for the higher mean shear rates at $x/D=40$ when the flow is supersonic.

Velocity profiles measured along the corner bisector in Fig. 8 (solid symbol distributions) indicate that the flow does not approach a separated condition in the relatively low momentum corner layer, even though the flow is developing in the presence of an increasing adverse pressure gradient. This behavior differs from that for supersonic laminar square duct flow, where recent predictions based on similar inlet conditions have shown that local flow separation and flow reversal will occur in the corner region at a streamwise location less than $x/D=20$ (Ref. 2).[2] Mach number profiles corresponding to the velocity profiles in Fig. 8 are shown in Fig. 9. From this figure it can be seen that the centerline Mach number decreases markedly along the length of the duct (from a value of 3.91 at the duct inlet to a value of 1.82 at $x/D=50$). The wall and corner bisector profiles at $x/D=40$ and 50 approximately coincide, except in the near-wall region where subsonic flow exists over a greater portion of the corner layer at $x/D=50$.

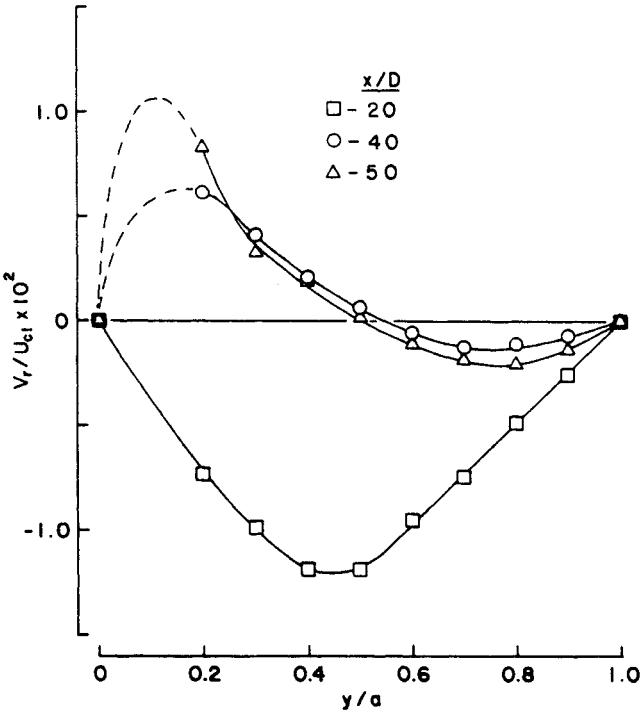

a) Wall bisector

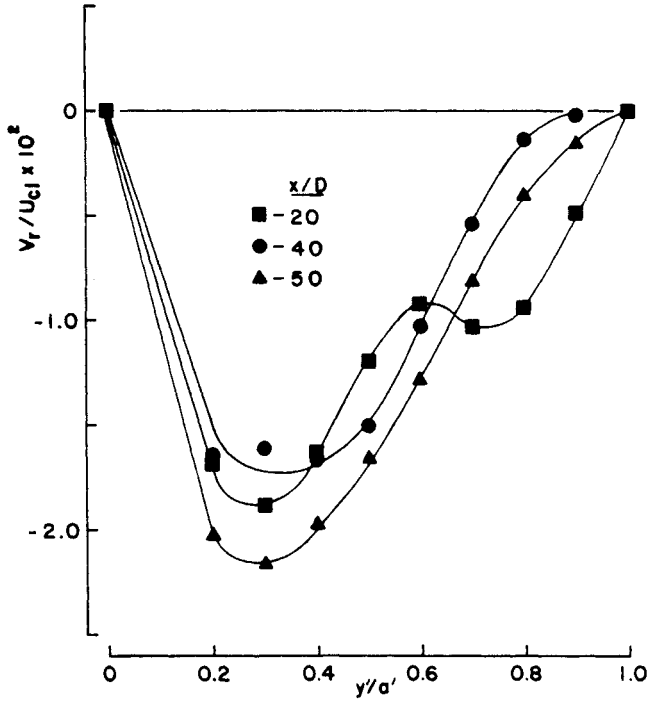

b) Corner bisector

Fig. 10 Transverse flow velocity profiles.

Secondary Flow Development

Transverse flow velocity profiles measured along the wall and corner bisector traverses at three streamwise locations ($x/D=20$, 40, and 50) are shown in Fig. 10. In reference to Fig. 10a, it can be seen that transverse flow along the wall bisector is directed initially toward the wall (V_r/U_{cl} is negative at $x/D=20$), until the secondary flow cells have grown to the extent that local flow reversal occurs, as indicated by the outwardly directed cross flow (V_r/U_{cl} positive) at $x/D=40$ and 50. This outwardly directed flow along the wall bisector at $x/D=50$ also can be seen in Fig. 5b. Figure 10b shows that

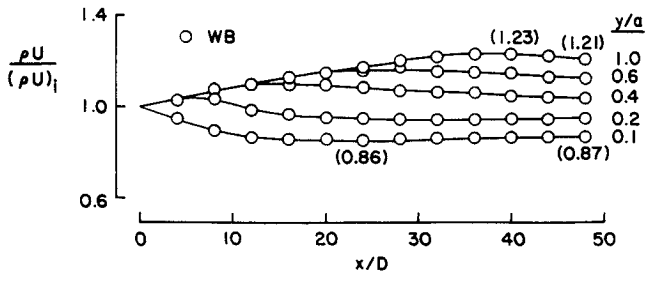

a) Incompressible case, $M_i = 0.05$ (Ref. 8)

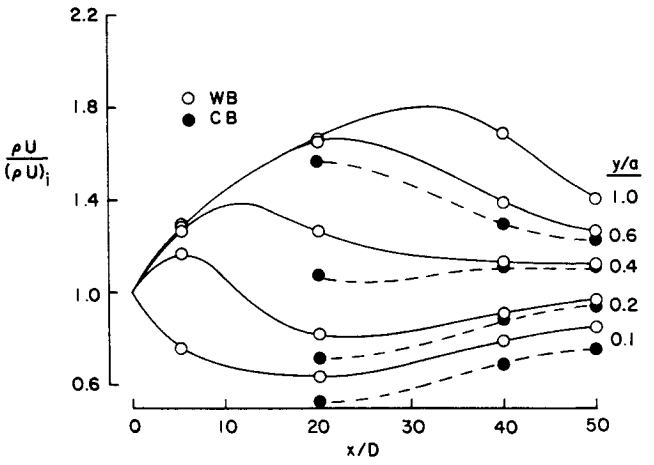

b) Supersonic case, $M_i = 3.9$

Fig. 11 Primary flow mass flux behavior.

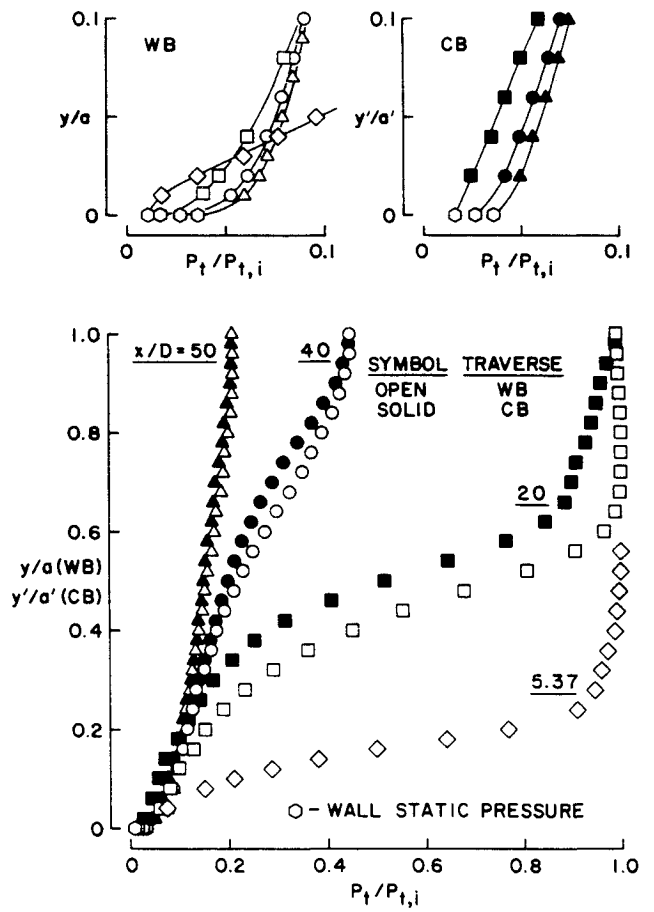

Fig. 12 Streamwise development of total pressure profiles.

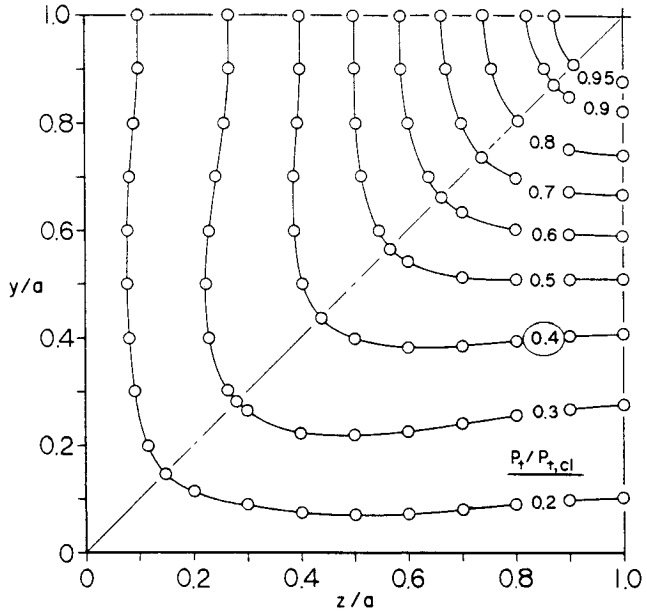

a) $x/D = 40$

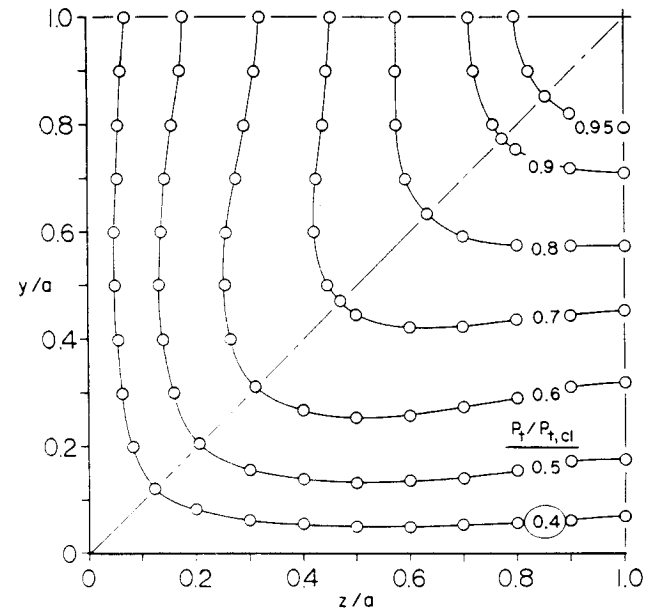

b) $x/D = 50$

Fig. 13 Total pressure contours.

transverse flow along the corner bisector at all three streamwise locations is always directed toward the corner, with a peak strength in the immediate vicinity of the corner.

Factors Influencing Flow Development

In order to analyze the relative importance of pressure gradient and secondary flow effects on local flow development more closely, the local mass flux was calculated at points along the wall and corner bisectors of the duct and compared with results previously obtained for the incompressible case. Figure 11 shows distributions of the primary flow (x-direction) mass flux at fixed distances from the wall for both cases. In the initial flow development region ($0 \leq x/D \leq 20$), the mass flux near the wall (e.g., at $y/a = 0.1$) decreases as a result of boundary-layer growth and streamline displacement away from the wall. The mass flux in the vicinity of the duct centerline (at $y/a = 1$) correspondingly increases in order to satisfy

continuity. This behavior is accentuated by the streamwise adverse pressure gradient when the flow is supersonic (compare the wall bisector distributions at $y/a=0.1$ and 1 between $x/D=0$ and 20 for both cases).

For the incompressible case, when the wall boundary layers initially merge (nominally at $x/D=30$), the transverse shear stress gradient on the duct centerline ($2\,\partial\overline{u'v'}/\partial y$) is less than the magnitude of the streamwise pressure gradient ($|\partial P/\partial x|$), so the flow continues to accelerate at this location by virtue of streamwise momentum considerations [$U\,\partial(\rho U)/\partial x$ is positive]. This leads to a local peaking of the mass flux on the duct centerline further downstream (near $x/D=40$, Fig. 11a), followed by a decrease as the flow continues to develop downstream. Associated with this behavior is a corresponding slight increase in mass flux levels near the wall in order to satisfy continuity. For the supersonic case (Fig. 11b), these trends are accentuated by the streamwise adverse pressure gradient, and mass flux levels near the wall (e.g., at $y/a=0.1$ and 0.2) increase significantly between $x/D=20$ and 50. This behavior implies that observed increases in other transferable properties near the wall between $x/D=20$ and 50 (such as mean-flow momentum or energy) can be attributed primarily to shear layer interaction effects, rather than to the convecting action of the secondary flow.

Results such as those shown in Figs. 12 and 13 can now be interpreted accordingly. Figure 12 shows total pressure profiles measured along the wall and corner bisectors of the duct at four streamwise locations, while Fig. 13 shows total pressure contours measured in a quadrant of the flow at $x/D=40$ and 50. In reference to the near-wall results shown in expanded form in Fig. 12, it can be seen that total pressure values at a given streamwise location approach the local wall static pressure in a consistent manner, which implies that wall and wave-reflection effects did not significantly affect total pressure measurements in the near-wall region. The expanded views also show that total pressure (mean-flow energy) levels continually increase between $x/D=20$ and 50. This behavior is similar to that observed in Fig. 11b for mass flux levels near the wall over the same interval and is directly attributable to the shear layer interaction. In the inviscid core region at $x/D=20$, Fig. 12 shows that total pressure values on the corner bisector deviate from the inlet total pressure level ($P_t/P_{t,i}<1$ for $0.7<y'/a'<1$). This behavior is the result of weak wave reflections in the duct that tend to lower total pressure levels in the vicinity of the corner bisector at this streamwise location (cf. Fig. 7b of Ref. 5). The effect of these weak waves on axial mean velocity values in the core region at $x/D=20$ is minimal, however, as is evident from the wall and corner bisector profiles shown in Fig. 8.

In reference to Fig. 13, it can be seen that total pressure contours at $x/D=40$ normalized by the centerline total pressure are qualitatively similar to those at $x/D=50$, except that contours of a given level lie closer to the wall at $x/D=50$ (compare the relative positions of the contour $P_t/P_{t,cl}=0.4$ in Figs. 13a and 14b). These shifts in contour position correspond to an increase in contour level at a given distance from the wall between $x/D=40$ and 50. This increase is not associated with an increase in strength of the secondary flow, which remains relatively constant between $x/D=40$ and 50 (refer to Fig. 10), but is due, instead, to mixing losses in the outer region of the boundary layer that lead to a reduction of total pressure in this region between $x/D=40$ and 50 (refer to Fig. 12). Since total pressure values in the near-wall region increase over this interval as a result of shear layer interaction effects, contour levels at a fixed distance from the wall must correspondingly increase, as shown in Fig. 13.

Near-Wall Flow Behavior

In order to investigate how well local law-of-the-wall behavior applies in both the streamwise and spanwise directions, local skin friction measurements were made with four different diameter Preston tubes, and the data were reduced by means of the calibration equation proposed by Bradshaw and Unsworth.[12] Spanwise distributions of C_f measured along the wall $y=0$ between the wall bisector ($z_c/a=0$, with z_c defined as shown in Fig. 7) and the corner ($z_c/a=1$) are shown in Fig. 14 for three streamwise locations ($x/D=20$, 40, and 50). The maximum error in calculated C_f values occurs at $x/D=40$, where the assumption that the axial centerline (boundary-layer edge) static pressure is equal to the wall static pressure, leads to a fixed error in calculated C_f values of 0.6%. The positions of local maxima in the distributions measured at $x/D=40$ and 50 in Fig. 14 correlate well with the point of minimum separation distance between the wall and the first adjacent total pressure contour shown in Fig. 13 at each location. The line distributions in Fig. 14 are drawn through average values for the three data sets at each streamwise location. These distributions were used to specify local friction velocity (U_τ) values in order to plot velocity profiles in terms of van Driest-scaled variables.

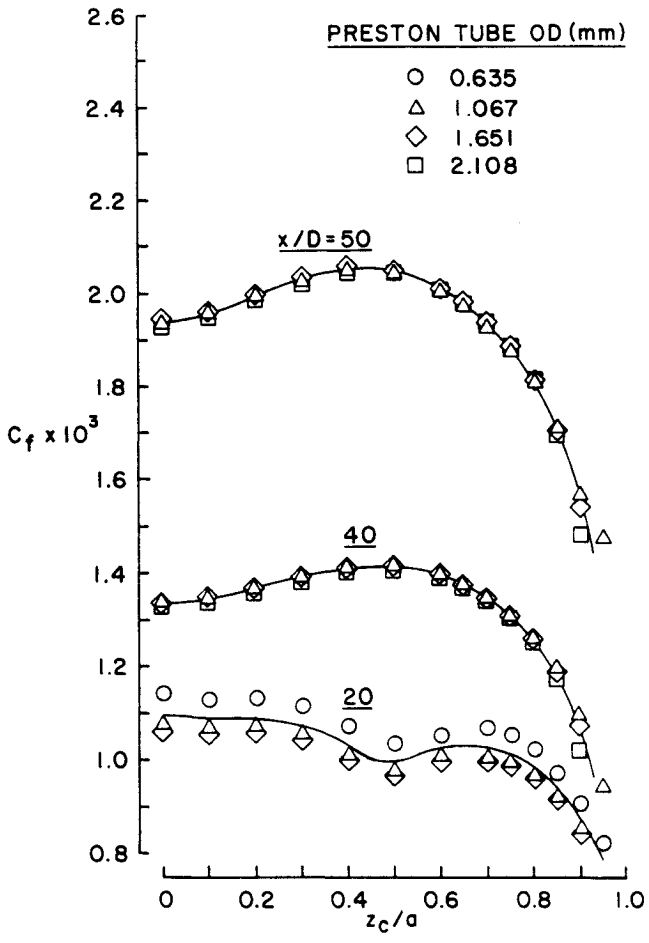

Fig. 14 Spanwise skin friction coefficient distributions.

Figure 15 shows axial velocity profiles along the wall bisector at $x/D=5.37$, 20, 40, and 50 plotted in terms of van Driest-scaled variables. Included in this figure are line distributions based on values for κ and C in the law-of-the-wall that provide the best fit to comparable profiles measured in incompressible square duct flow.[4] Also shown are d^+ values corresponding to the outside diameter of the Preston tubes used to determine the local friction velocity at each streamwise location. From the figure it is evident that the experimental results lie slightly, but consistently, above the law-of-the-wall (solid line) distribution in the log-law region. This behavior is not attributable to adverse pressure gradient effects, inasmuch as values of the local pressure gradient parameter, β_κ, were always less than 0.11, which is close to the value that applies for supersonic, adiabatic-wall, flat plate flow ($\beta_\kappa=0$).[13] The

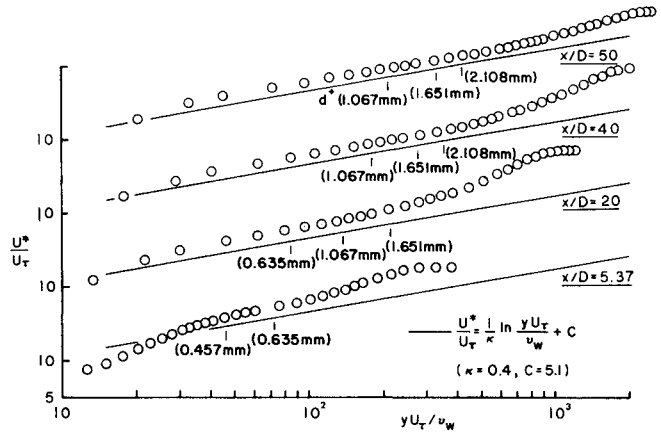

Fig. 15 Axial mean velocity profiles along the wall bisector.

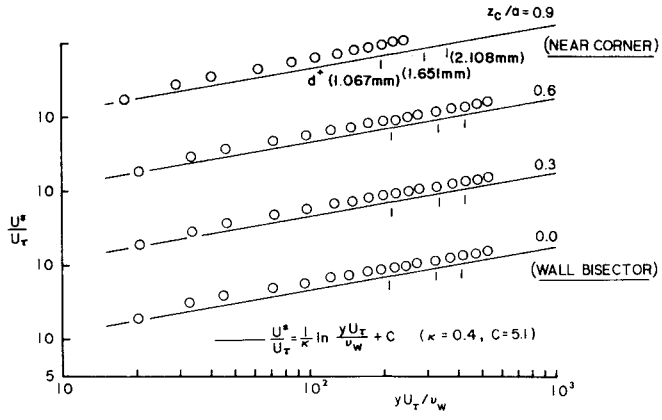

Fig. 16 Axial mean velocity profiles in the near-wall region at $x/D=50$.

observed differences are attributable, instead, to a slight underestimation of local friction velocity values (by approximately 10%) when the calibration equation proposed by Bradshaw and Unsworth[12] is used to reduce Preston tube data taken in supersonic flow. Further justification for this conclusion is given in Ref. 5.

Figure 15 also shows that the wake component of the velocity profile increases between $x/D=5.37$ and 20, which is in accord with anticipated behavior, but then decreases between $x/D=40$ and 50. This behavior can be explained by noting that the wake component at $x/D=40$ is accentuated by shear-layer interaction effects that tend to increase axial mean velocity gradients (velocity changes) in the outer region of the flow. The lessening of this effect downstream apparently overrides the influence of a slightly increasing adverse pressure gradient between $x/D=40$ and 50 that, in itself, would tend to increase the wake component between these two locations.

Velocity profiles measured at $x/D=50$ near the wall $y=0$ at four different spanwise locations between the corner and wall bisector are shown in Fig. 16 in terms of van Driest-scaled variables. The results for $z_c/a=0$, 0.3, and 0.6 extend to $y/a=0.2$, whereas the results for $z_c/a=0.9$ are terminated at $y/a=0.1$. From the figure it is evident that local law-of-the-wall behavior extends well into the corner region, even though the wall shear stress is varying locally over the span of the duct (refer to Fig. 14). The results in Figs. 15 and 16 demonstrate the existence of near-wall similarity over a development length longer than that considered in previous related work ($0\leq x/D\leq 20$; see Ref. 5) and are compatible with results previously obtained in incompressible square duct flow.[4]

Conclusions

Steady, supersonic, turbulent, adiabatic-wall flow in a square duct has been investigated over a development length from $x/D=0$ to 50 for a uniform flow, Mach 3.9 inlet condition. The results indicate that local flow development is sensitive to shear layer interaction effects that are enhanced by the streamwise adverse pressure gradient. The secondary flow develops in a manner similar to that observed for the incompressible case and serves primarily to distort the primary flow. Axial mean velocity profiles plotted in terms of van Driest-scaled variables exhibit log-law behavior in the near-wall layer. This result implies that wall functions used to calculate incompressible streamwise corner flows, when suitably modified for compressible flow, also may be applied to supersonic corner flows.

The results generated in the present study characterize a supersonic square duct flow that develops in an environment free of strong shock waves induced by compression surface or leading-edge effects. As such, the data reflect viscous interactions in the flow and, in particular, the effects of a turbulence-driven secondary flow, rather than being dominated by an inviscid shock structure associated with ramp or compression effects. The data thus illustrate the physical features of a "pure" supersonic corner flow and constitute a particularly stringent test for turbulence models that have been proposed, or are currently applied, to predict supersonic corner flows.

Acknowledgment

This study was sponsored by the NASA-Ames Research Center, Moffett Field, California, under Interchange Agreement No. NCA2-1R850-401.

References

[1]Davis, F. O., Gessner, F. B., and Kerlick, G. D., "Experimental and Numerical Investigation of Supersonic Turbulent Flow Through a Square Duct," *AIAA Journal,* Vol. 24, Sept. 1986, pp. 1508-1515.

[2]Davis, D. O., Gessner, F. B., and Kerlick, G. D., "Supersonic Laminar Flow Development in a Square Duct," *AIAA Journal,* Vol. 25, Jan. 1987, pp. 175-177.

[3]Melling, A., "Investigation of Flow in Non-Circular Ducts and Other Configurations by Laser Doppler Anemometry," Ph. D. Thesis, Univ. of London, London, 1975; see also *Journal of Fluid Mechanics,* Vol. 78, Pt. 2, 1976, pp. 289-315.

[4]Lund, E. G., "Mean Flow and Turbulence Characteristics in the Near Corner Region of a Square Duct," M. S. Thesis, Dept. of Mechanical Engineering, Univ. of Washington, Seattle, WA, 1977.

[5]Gessner, F. B., Ferguson, S. D., and Lo, C. H., "Experiments on Supersonic Turbulent Flow Development in a Square Duct," *AIAA Journal,* Vol. 25, May 1987, pp. 690-697.

[6]Lo, C. H., "Mean Flow Measurements in a Square Duct for Supersonic Turbulent Flow Conditions," M. S. Thesis, Dept. of Mechanical Engineering, Univ. of Washington, Seattle, WA, 1982.

[7]Davis, D. O., "Experimental and Numerical Investigation of Steady, Supersonic, Turbulent Flow Through a Square Duct," M.S. Thesis, Dept. of Mechanical Engineering, Univ. of Washington, Seattle, WA, 1985.

[8]Gessner, F. B., Po, J. K., and Emery, A. F., "Measurements of Developing Turbulent Flow in a Square Duct," *Turbulent Shear Flows I,* edited by F. Durst, B. E. Launder, F. W. Schmidt, and J. H. Whitelaw, Springer-Verlag, New York, 1979, pp. 119-136.

[9]Keenan, J. H. and Neumann, E. P., "Measurements of Friction in a Pipe for Subsonic and Supersonic Flow of Air," *Journal of Applied Mechanics,* Vol. 68, June 1946, pp. A91-A100.

[10]Om, D., "Static Pressure Measurements in the Regions of Adverse Pressure Gradient in Supersonic Flow," Dept. of Mechanical Engineering, Univ. of Washington, Seattle, WA, Report UW-ME-TR-78-GA-5-1, 1978.

[11]Gessner, F. B. and Emery, A. F., "The Numerical Prediction of Developing Turbulent Flow in Rectrangular Ducts," *Journal of Fluids Engineering,* Vol. 103, No. 3, Sept. 1981, pp. 445-455.

[12]Bradshaw, P. and Unsworth, K., "Comment on Evaluation of Compressible-Flow Preston Tube Calibrations," *AIAA Journal,* Vol. 12, Sept. 1974, pp. 1293-1295.

[13]Lewis, J. E., Gran, R. L., and Kubota, T., "An Experiment on the Adiabatic Compressible Turbulent Boundary Layer in Adverse and Favorable Pressure Gradients," *Journal of Fluid Mechanics,* Vol. 51, Pt. 4, 1972, pp. 657-672.